Journal of Sound and Vibration (1998) **209**(2), 251–264

FRICTION-INDUCED PARAMETRIC RESONANCES IN DISCS: EFFECT OF A NEGATIVE FRICTION-VELOCITY RELATIONSHIP

H. OUYANG AND J. E. MOTTERSHEAD

Department of Mechanical Engineering, University of Liverpool, Liverpool L69 3GH, England

M. P. CARTMELL

Department of Mechanical Engineering, University of Edinburgh, Edinburgh, EH9 3JL, Scotland

AND

M. I. FRISWELL

Department of Mechanical Engineering, University of Wales Swansea, Swansea SA2 8PP, Wales

(*Received* 3 *July* 1996, *and in final form* 25 *April* 1997)

Parametric resonances are studied which occur when an elastic system is rotated around an annular disc with friction having a negative slope with velocity. The elastic system consists of two spring–dashpots, in the transverse and in-plane (circumferential) directions, and a common point mass. The complete arrangement is driven around the disc through the in-plane stiffness and damper. It is demonstrated that the effect of the in-plane system (including the negative friction–velocity relationship) is (i) to introduce additional parametric resonances which are destabilised by the transverse damper, and (ii) to reduce the regions of instability of the other resonances.

1. INTRODUCTION

The instabilities that occur above the critical speed when either (i) a transverse mass–spring–damper system is rotated around a stationary flexible disc, or (ii) a disc is rotated past a stationary *m-k-c* system have been studied in considerable detail by Mote [1, 2], Iwan and Stahl [3], Iwan and Moeller [4], Hutton *et al*. [5], Shen and Mote [6, 7] and Shen [8]. Ono *et al*. [9], Chen and Bogy [10] and Mottershead and Chan [11] investigated the speed-independent instabilities that were induced by a frictional follower force. Chan *et al*. [12] and Mottershead *et al*. [13] calculated the instability regions for subcritical-speed parametric resonances in discs with transverse loads and a constant dynamic coefficient of friction. The review article by Mottershead [14] gives a thorough account of research in the field.

The models of friction that have variously been derived from the mathematical physics or from empirical relationships have been studied with the particular purposes of numerical analysis (Oden and Martins [15]), automatic control (Armstrong-Helouvry [16]) and non-linear dynamics (Ibrahim, [17, 18]). One well-known aspect of friction in dynamic systems is the instability that accompanies a friction force that falls as the relative velocity increases. The previous investigations into combinational instabilities in discs [1–13]

0022–460X/98/020251 + 14 $25.00/0/sv971261

offered no opportunity to study the friction–velocity effect because the transverse *m*-*k*-*c* system was rotated at constant speed relative to the disc. In reference [13] the authors determined the instability regions in an elastic disc with a rotating system of mass, stiffness, damping and friction distributed over an annular sector; like the brake pad in a vehicle disc brake. Another feature of disc brakes is in-plane flexibility of the pad due in part to the shear-stiffness of the pad material and also to flexibilities in the calliper and its mounting arrangement. At very low speeds the in-plane flexibility leads to stick–slip behaviour which couples with the transverse motion through the friction force (Ouyang *et al*. [19]) and can give rise to instabilities known in the industry as 'brake groan'. In the present article speeds are considered that are high enough to prevent sticking but which are entirely in the range of the negative friction–velocity relationship for the materials concerned. It is shown that the parametric resonances previously determined for a system with a constant coefficient of friction [12] remain, and tend to be stabilized by the in-plane system with a negative-sloping friction. In addition, new parametric resonances appear which can be destabilised by damping in the transverse part of the rotating *m*-*k*-*c* system. This latter (counter-intuitive) result is new and in agreement with experience reported in the brakes industry which until now has lacked a scientific explanation.

The analysis is conservative in that it presents the most serious case of friction with a negative slope. At higher speeds in a physical system it is possible that the direction of the slope may have changed to become positive, in which case the in-plane oscillations will be damped out and the analysis presented in this article should be reduced to that of Chan *et al*. [12]. The very high speed effects are almost of no practical interest in vehicle brakes, which was the principal motivation for this study.

2. FRICTION MODEL

When a mass is driven through a spring at low speeds across a dry surface the resulting motion of the mass will be that of consecutive sliding and sticking—usually known as stick–slip. At a sufficiently high speed the spring force always exceeds the frictional capacity and the mass will then be in a condition of permanent sliding. In what follows it is assumed there to be no stick phase in the motion, which means that the discontinuous (stick–slip) non-linearity disappears from the equations, rendering them tractable by perturbation analysis. The friction force developed in driving a mass through a spring around a circular path is assumed to take the form

$$F_\theta = \tilde{F}_\theta\,[1 - \alpha(\dot{\varphi} + \tilde{\Omega})], \tag{1}$$

where $\tilde{\Omega}$ is the constant angular speed at the driven end of the spring, $\dot{\varphi}$ is the velocity of the mass relative to the driving speed, $\tilde{F}_\theta$ is the product of the normal force and the static coefficient of friction, and α is a positive constant which defines the negative slope of F_θ against the angular speed of the mass $(\dot{\varphi} + \tilde{\Omega})$.

3. THE LOADED DISC ARRANGEMENT

A mass, spring, damper arrangement is driven with friction around an annular disc. The arrangement consists of two spring–dashpot systems, in the transverse and in-plane (circumferential) directions, and a common point mass. The mass remains in contact with the disc and traces a circle of radius r_0 on the disc's surface. The arrangement of the mass, springs and dampers is illustrated in Figure 1, where it is shown that a constant angular speed, $\tilde{\Omega}$, is applied at one end of the in-plane system (k_p, c_p) while the mass and the transverse system, (k, c), being attached at the other end, may have a velocity $(\dot{\varphi} + \Omega)$.

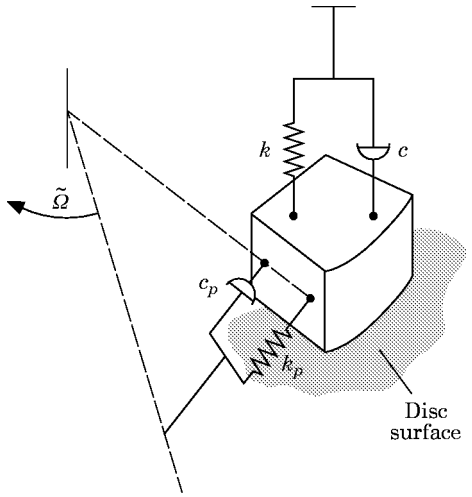

Figure 1. Transverse and in-plane load arrangement.

Thus it is the in-plane spring–dashpot which permits the friction force to vary according to equation (1), and the complete in-plane system can be regarded as consisting of k_p, c_p and the negative friction–velocity relationship. Now consider F_θ to act as a follower force, as shown in Figure 2, which has the effect of coupling the transverse and in-plane motions.

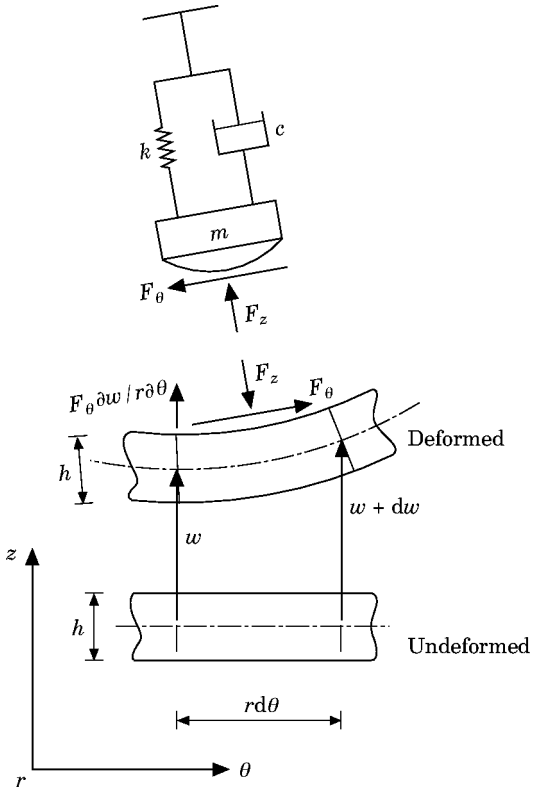

Figure 2. Frictional follower force.

The differential equations governing motion in the two directions can be written as follows: (a) in-plane motion,

$$r_0\,(m\ddot{\varphi} + c_p\,\dot{\varphi} + k_p\,\varphi) = -F_\theta = -\tilde{F}_\theta\,[1 - \alpha(\dot{\varphi} + \tilde{\Omega})], \tag{2}$$

and (b) transverse motion,

$$\begin{aligned}\rho h\,\partial^2 w/\partial t^2 + D^*\nabla^4\partial w/\partial t + D\nabla^4 w = {} & -(1/r)\,\delta(r - r_0)\,\delta(\theta - \varphi - \tilde{\Omega}t)\\ & \times \{m[\ddot{\varphi}\,\partial w/\partial\theta + (\dot{\varphi} + \tilde{\Omega})^2\,\partial^2 w/\partial\theta^2 + 2(\dot{\varphi} + \tilde{\Omega})\,\partial^2 w/\partial\theta\,\partial t + \partial^2 w/\partial t^2]\\ & + c[(\dot{\varphi} + \tilde{\Omega})\,\partial w/\partial\theta + \partial w/\partial t] + kw - \tilde{F}_\theta\,[1 - \alpha(\dot{\varphi} + \tilde{\Omega})]\,\partial w/r\partial\theta\},\end{aligned} \tag{3}$$

where ρ, h, D and D^* represent the density, thickness, flexural rigidity and flexural damping of the disc respectively. The displacement, w, of the disc is identically the transverse displacement of the mass at the point indicated by the two Dirac delta functions. The overdots denote differentiation with respect to time, and ∇^4 is the biharmonic operator in polar co-ordinates. One can observe from equations (2) and (3) that there is a 'one-way' coupling between the in-plane and transverse vibrations of the mass. Specifically, φ can be solved for from equation (2) independently of w, but w can be determined from equation (3) only when φ is known.

4. IN-PLANE MOTION

Equation (2) can be re-written in the form,

$$\ddot{\varphi} + (1/m)\,(c_p - \tilde{F}_\theta\,\alpha/r_0)\dot{\varphi} + \omega_p^2\,\varphi = -\tilde{F}_\theta\,(1 - \alpha\tilde{\Omega})/mr_0, \tag{4}$$

where $\omega_p = \sqrt{(k_p\,/m)}$ is the undamped natural frequency of the in-plane system. One can distinguish three cases for transient response to the in-plane system which depend on different values of the 'damping' term $(c_p - \tilde{F}_\theta\,\alpha/r_0)$: (a) when $c_p < \tilde{F}_\theta\,\alpha/r_0$ the damping would be negative and the oscillations would grow to cause the onset of stick-slip motion (which is not covered in this article); (b) when $c_p > \tilde{F}_\theta\,\alpha/r_0$ the in-plane vibrations would be damped out so that the disc mass rotates steadily around the disc at the driving speed $\tilde{\Omega}$ (which reduces to the condition already studied by Chan *et al*. [12]); and (c) when $\tilde{F}_\theta\,\alpha/r$ is smaller than, yet close to c_p, a condition of persistent harmonic oscillations can be set up in the system. The latter of the three cases above is chosen to be studied, and in doing so a small parameter ε is defined such that $2\varepsilon\zeta_p\,\omega_p = (1/m)\,(c_p - \tilde{F}_\theta\,\alpha/r_0)$, where ζ_p is the equivalent damping ratio of the in-plane system. Then with the initial conditions, $\varphi|_{t=0} = \varphi_0 = -\tilde{F}_\theta\,/k_p\,r_0$ and $\dot{\varphi}|_{t=0} = 0$, it is found that

$$\varphi(t) = \varphi_0\,\{(\alpha\tilde{\Omega}/2)\,[\exp(\mathrm{i}\omega_p\,t) + \exp(-\mathrm{i}\omega_p\,t)] + 1 - \alpha\tilde{\Omega}\} + O(\varepsilon), \tag{5}$$

and (upon differentiating) that $(\dot{\varphi} + \tilde{\Omega}) > 0$ when $\alpha\varphi_0\,\omega_p < 1$. The physical significance of this condition is that the friction force never reverses its direction and the mass continues to slide in one direction around the disc without sticking. This condition is assumed to hold throughout the analysis in the present article.

5. TRANSVERSE MOTION

The solution of equation (4) is supposed to take the form (Chan *et al*. [12]),

$$w(r, \theta, t) = \sum_{r=0}^{\infty}\sum_{s=-\infty}^{\infty}\psi_{rs}\,(r, \theta)q_{rs}\,(t), \qquad \psi_{rs}\,(r, \theta) = (1/\sqrt{\rho hb^2})R_{rs}\,(r)\exp(\mathrm{i}s\theta), \tag{6, 7}$$

where r and s denote the number of nodal circles and diameters respectively, q_{rs} is a modal co-ordinate and ψ_{rs} is a complex eigenfunction. $R_{rs}(r)$ is a combination of Bessel functions satisfying the boundary conditions (on the inner and outer circumferences) and the orthonormality conditions [12]. Combining equations (5–7) with equation (3) (but omitting the $O(\varepsilon)$ term in equation (5)) leads to

$$\frac{\mathrm{d}^2 q_{kl}}{\mathrm{d}\tau^2} + \frac{D^* \omega_{cr}\, \beta_{kl}^2}{D} \frac{\mathrm{d}q_{kl}}{\mathrm{d}\tau} + \beta_{kl}^2\, q_{kl} = -\sum_{r=0}^{\infty} \sum_{s=-\infty}^{\infty} R_{rs}(r_0) R_{kl}(r_0) \exp[\mathrm{i}(s-l)\Omega\tau]$$

$$\times \left\{ \frac{m}{\rho h b^2} \left\{ \frac{\mathrm{d}^2 q_{rs}}{\mathrm{d}\tau^2} + s\Omega[2\mathrm{i} + \alpha\varphi_0\, \omega_p (\exp(-\mathrm{i}\beta_p\, \tau) - \exp(\mathrm{i}\beta_p\, \tau))] \frac{\mathrm{d}q_{rs}}{\mathrm{d}\tau} - s^2\Omega^2 \right.\right.$$

$$\times \left[\frac{\mathrm{i}\alpha\varphi_0\, \omega_p}{2} (\exp(\mathrm{i}\beta_p\, \tau) - \exp(\mathrm{i}\beta_p\, \tau)) + 1 \right]^2 q_{rs} - \frac{\mathrm{i}s\alpha\varphi_0\, \omega_p^2\, \Omega}{2\omega_{cr}}$$

$$\left.\left. \times (\exp(-\mathrm{i}\beta_p\, \tau) + \exp(\mathrm{i}\beta_p\, \tau)) q_{rs} \right\} + \frac{c}{\rho h b^2 \omega_{cr}} \left\{ \frac{\mathrm{d}q_{rs}}{\mathrm{d}\tau} + \mathrm{i}s\Omega \right.\right.$$

$$\left.\left. \times \left[\frac{\mathrm{i}\alpha\varphi_0\, \omega_p}{2} (\exp(\mathrm{i}\beta_p\, \tau) - \exp(\mathrm{i}\beta_p\, \tau)) + 1 \right] q_{rs} \right\} + \frac{k}{\rho h b^2 \omega_{cr}^2}\, q_{rs} \right.$$

$$\left. - \frac{\mathrm{i}s\tilde{F}_\theta}{\rho h b^2 r_0\, \omega_{cr}^2} \left\{ 1 - \alpha\tilde{\Omega} \left[\frac{\mathrm{i}\alpha\varphi_0\, \omega_p}{2} (\exp(\mathrm{i}\beta_p\, \tau) - \exp(-\mathrm{i}\beta_p\, \tau)) + 1 \right] q_{rs} \right\} \right\}, \tag{8}$$

where φ is assumed to be small, so $(\varphi + \tilde{\Omega}t) \approx \tilde{\Omega}t$, and the following non-dimensional variables have been introduced:

$$\tau = \omega_{cr}\, t, \qquad \beta_{kl} = \omega_{kl}/\omega_{cr}, \qquad \beta_p = \omega_p/\omega_{cr}, \qquad \Omega = \tilde{\Omega}/\omega_{cr}. \tag{9–12}$$

The klth natural frequency is denoted by ω_{kl}, and ω_{cr} is the first critical speed of the disc. A multiple-scales analysis including terms to $O(\varepsilon)$ is carried out in the following section.

6. MULTIPLE SCALES ANALYSIS

The small parameter ε is used to re-define the terms of the disc and the load system:

$$\varepsilon\gamma = m/\rho h b^2, \qquad \varepsilon\kappa = k/\rho h b^2 \omega_{cr}^2, \qquad \varepsilon\zeta = c/\rho h b^2 \omega_{cr}, \tag{13–15}$$

$$\varepsilon\xi = D^*/D\omega_{cr}, \qquad \varepsilon f = \tilde{F}/\rho h b^2 r_0\, \omega_{cr}^2. \tag{16, 17}$$

By following the usual procedures (Nayfeh and Mook [20], Shen [8], Chan *et al*. [12]) one obtains the zeroth and first order contributions to the modal co-ordinates from

$$q_{kl}^{(0)} = A_{kl}(T_1) \exp(\mathrm{i}\beta_{kl}\, T_0) + B_{kl}(T_1) \exp(-\mathrm{i}\beta_{kl}\, T_0), \tag{18}$$

and

$$D_0^2\, q_{kl}^{(1)} + \beta_{kl}^2\, q_{kl}^{(1)} = -D_0 (2D_1 + \xi\beta_{kl}^2) [A_{kl} \exp(\mathrm{i}\beta_{kl}\, T_0) + B_{kl} \exp(-\mathrm{i}\beta_{kl}\, T_0)] + Y_1(\gamma, \kappa, \zeta, f(1 - \alpha\tilde{\Omega})) + Y_2(\gamma, \zeta, f, k_p), \tag{19}$$

TABLE 1

Natural frequencies of the disc

r, s	0, 0	0, 1	0, 2	0, 3	0, 4
ω_{rs} (rad/s)	28598	29396	32437	39434	52482
ω_{rs}	2·1796	2·2404	2·4722	3·0055	4

where

$$Y_1(\gamma, \kappa, \zeta, f) = -\sum_{r=0}^{\infty}\sum_{s=-\infty}^{\infty} R_{kl}(r_0)R_{rs}(r_0)\exp[\mathrm{i}(s-l)\Omega T_0] \times [D_{rs}^{+} A_{rs}\exp(\mathrm{i}\beta_{rs} T_0) + D_{rs}^{-} B_{rs}\exp(-\mathrm{i}\beta_{rs} T_0)], \tag{20}$$

$$D_{rs}^{+} = -\gamma[(C_{rs}^{+})^2 + (s\Omega\alpha\varphi_0\omega_p)^2/2] + \mathrm{i}(\zeta C_{rs}^{+} - sf) + \kappa, \qquad C_{rs}^{+} = \beta_{rs} + s\Omega, \tag{21, 22}$$

$$D_{rs}^{-} = -\gamma[(C_{rs}^{-})^2 + (s\Omega\alpha\varphi_0\omega_p)^2/2] - \mathrm{i}(\zeta C_{rs}^{-} + sf) + \kappa, \qquad C_{rs}^{-} = \beta_{rs} - s\Omega, \tag{23, 24}$$

are the terms reported by Chan *et al*. [12], except that the second term in the square brackets of equations (21) and (23) is introduced by the negative sloping friction, and

$$\begin{aligned} Y_2(\gamma, \zeta, f, k_p) = -\sum_{r=0}^{\infty}\sum_{s=-\infty}^{\infty} & s\Omega\alpha\varphi_0\omega_p R_{kl}(r_0)R_{rs}(r_0)\exp[\mathrm{i}(s-l)\Omega T_0] \\ & \times \{\{\mathrm{i}\gamma s\Omega + [(\zeta + f\alpha\omega_{cr})/2]\}[\exp(-\mathrm{i}\beta_p T_0) - \exp(\mathrm{i}\beta_p T_0)] \\ & - (\mathrm{i}\gamma\beta_p/2)[\exp(\mathrm{i}\beta_p T_0) + \exp(-\mathrm{i}\beta_p T_0)] + (\gamma s\Omega\alpha\varphi_0\omega_p/4)[\exp(\mathrm{i}2\beta_p T_0) \\ & + \exp(-\mathrm{i}2\beta_p T_0)]\}[A_{rs}\exp(\mathrm{i}\beta_{rs} T_0) + B_{rs}\exp(-\mathrm{i}\beta_{rs} T_0)] \\ & + \mathrm{i}\gamma\beta_{rs}[\exp(-\mathrm{i}\beta_p T_0) - \exp(\mathrm{i}\beta_p T_0)][A_{rs}\exp(\mathrm{i}\beta_{rs} T_0) \\ & - B_{rs}\exp(-\mathrm{i}\beta_{rs} T_0)]\} \end{aligned} \tag{25}$$

are the terms that appear only when the in-plane spring–dashpot and the negative friction velocity relationship are present. They have not been reported previously and produce unstable combination resonances involving β_p. The resonances that occur as combinations with the form $(s+l)\Omega \approx \pm\beta_{rs} - \beta_{kl}$ are modified by the in-plane spring–dashpot and the negative friction velocity relationship, whereas those having the forms $(s \pm l)\Omega \approx \pm\beta_{rs} \pm \beta_{kl} \pm \beta_p$ (including $2l\Omega \approx \beta_p$ and $2l\Omega \approx 2\beta_{kl} - \beta_p$) or $(s \pm l)\Omega \approx \pm\beta_{rs} \pm \beta_{kl} \pm 2\beta_p$ (including $2l\Omega \approx 2\beta_p$ and $2l\Omega \approx 2\beta_{kl} - 2\beta_p$) are initiated by the in-plane system.

The regions of instability for the modified combination parametric resonances are determined by a straightforward extension of the analysis by Chan *et al*. [12]. The stability analysis for three of the combination parametric resonances initiated by the in-plane system is presented in the Appendix.

7. SIMULATED EXAMPLES

A disc is considered with a clamped inner- and a free outer-radius $a = 0{\cdot}067$ m and $b = 0{\cdot}12$ m respectively. The rotating elastic system is located at a radius $r_0 = 0{\cdot}1$ m. The disc has Young's modulus $E = 1{\cdot}2 \times 10^5$ MPa, Poisson's ratio $v = 0{\cdot}25$, density

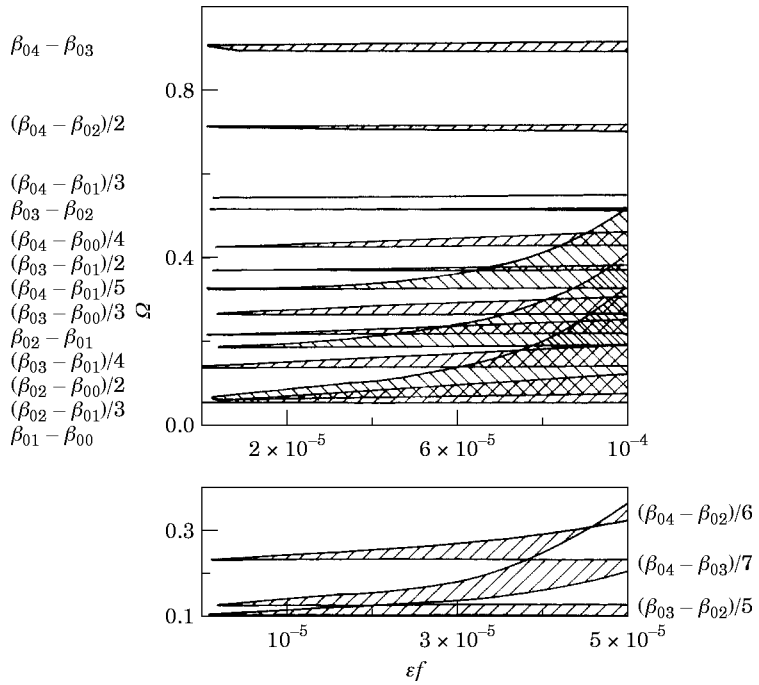

Figure 3. Instability regions for the system having no in-plane spring damper: dependence on friction. $\varepsilon\gamma = 0{\cdot}24$, $\varepsilon\kappa = 0{\cdot}7$, $\varepsilon\zeta = 5 \times 10^{-5}$, $\varepsilon\xi = 0$.

$\rho = 7000\,\mathrm{kgm}^{-3}$ and thickness $h = 0{\cdot}02$ m. The values taken for the parameters are $\varepsilon\gamma = 0{\cdot}24$, $\varepsilon\zeta = 5 \times 10^{-5}$, $\varepsilon\xi = 5 \times 10^{-13}$, $\varepsilon\kappa = 0{\cdot}7$, $\varepsilon f = 10^{-5}$, $\alpha = 3 \times 10^{-5}$ and $k_p = 5 \times 10^6$, which are reasonably representative of a production disc-brake. The value chosen for k_p is about one fifth of the value of the transverse stiffness k. The natural frequencies of the disc are given in Table 1.

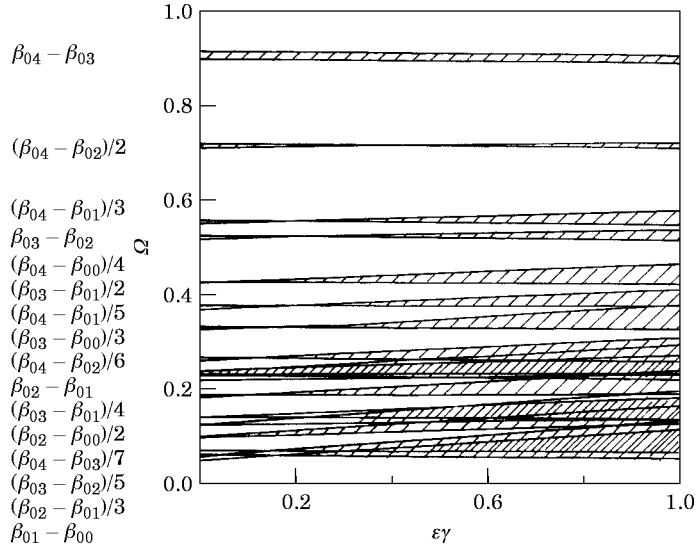

Figure 4. As Figure 3 but dependence on mass. $\varepsilon\kappa = 0{\cdot}7$, $\varepsilon\zeta = 5 \times 10^{-5}$, $\varepsilon\xi = 0$, $\varepsilon f = 10^{-5}$.

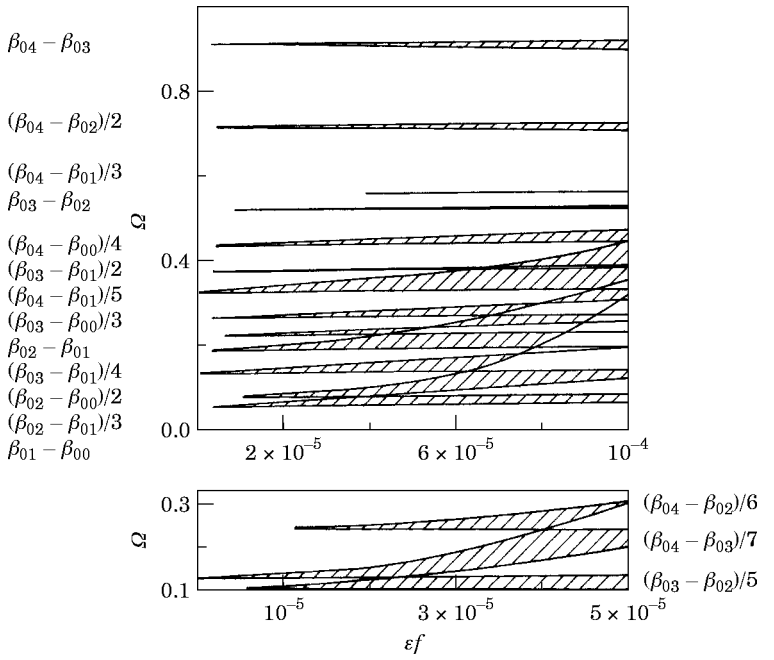

Figure 5. Modified instability regions: dependence on friction. $\varepsilon\gamma = 0{\cdot}24$, $\varepsilon\kappa = 0{\cdot}7$, $\varepsilon\zeta = 5 \times 10^{-5}$, $\varepsilon\xi = 0$, $\alpha = 3 \times 10^{-5}$, $k_p = 5 \times 10^{6}$.

7.1. MODIFIED RESONANCES

One can observe from equations (19–24) that the modification is principally concerned with the mass and friction parameters γ and f. Figures 3 and 4 show the dependence of the instability regions (shaded) on mass and friction with the in-plane spring–dashpot

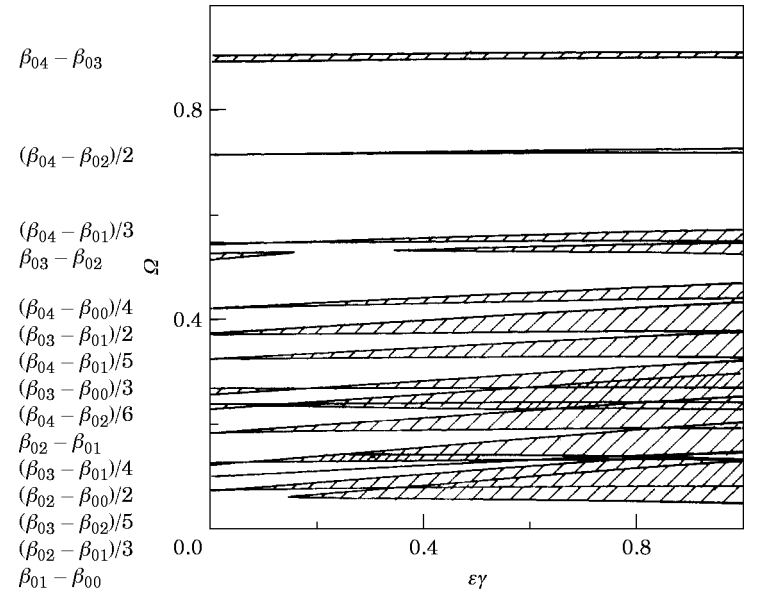

Figure 6. Modified instability regions: dependence on mass. $\varepsilon\kappa = 0{\cdot}7$, $\varepsilon\zeta = 10^{-5}$, $\varepsilon\xi = 0$, $\varepsilon f = 10^{-5}$, $\alpha = 3 \times 10^{-5}$, $k_p = 5 \times 10^{6}$.

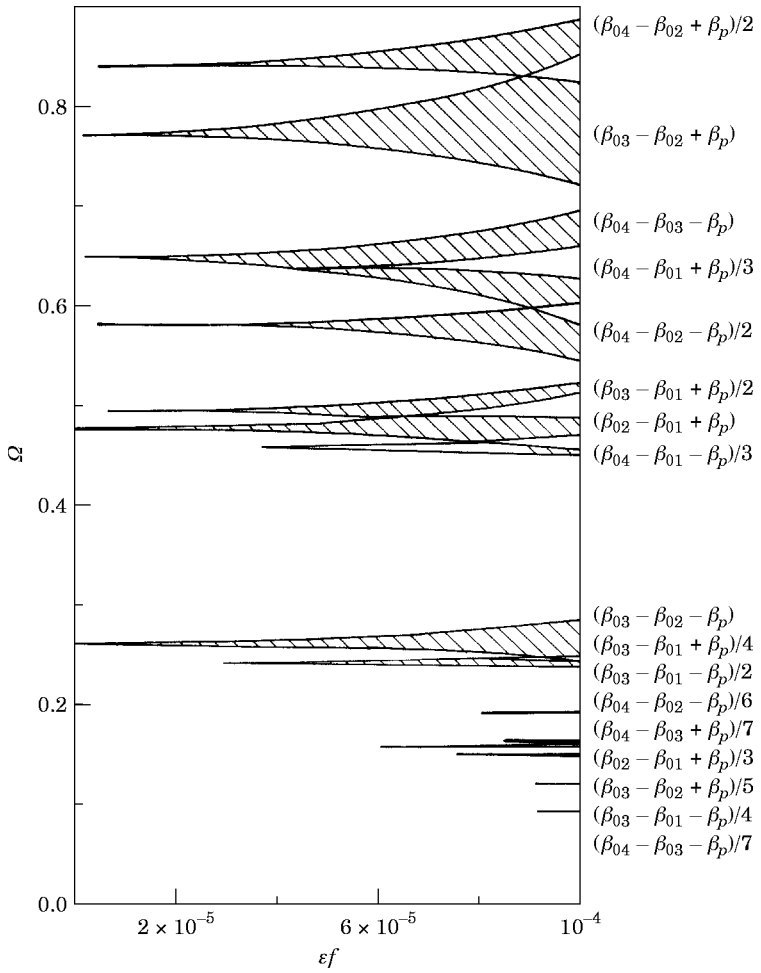

Figure 7. Instability regions initiated by the in-plane system: dependence on friction εf. $\varepsilon\gamma = 0{\cdot}24$, $\varepsilon\kappa = 0{\cdot}7$, $\varepsilon\zeta = 5 \times 10^{-5}$, $\varepsilon\xi = 5 \times 10^{-13}$, $\alpha = 3 \times 10^{-5}$, $k_p = 5 \times 10^6$.

removed. When the in-plane system is present then the instabilities are modified as shown in Figures 5 and 6. It can be seen that the modified resonances have smaller instability regions, which shows that the in-plane spring–dashpot and the negative friction velocity relationship have a stabilizing effect. Figures 3 and 5 are each drawn in two parts because the resonances $(\beta_{04} - \beta_{02})/6$, $(\beta_{04} - \beta_{03})/7$, and $(\beta_{03} - \beta_{02})/5$ are dominant and would obscure the instability regions of the other resonances if they were not drawn separately. The stabilizing effect of the in-plane system is seen most clearly in the three dominant instabilities. The in-plane stiffness k_p was found to have a neutral effect on the modified instability regions, which means that the differences between Figures 3 and 5 are mainly attributable to the negative friction–velocity relationship.

7.2. RESONANCES INITIATED BY THE IN-PLANE SYSTEM

The instability regions and their dependence on the parameters εf, $\varepsilon\zeta$, $\varepsilon\gamma$ and k_p are shown in Figures 7–10. Friction is clearly destabilizing. From equation (25) (or from equations (A5) and (A6) or equation (A9)) it is seen that the qualitative effect of the transverse damper must be the same as the friction, which explains the counter-intuitive

result shown in Figure 8. It has been known for some time, from experience in the vehicle brakes industry, that an increase in damping can be destabilizing, but it seems that the present analysis is the first to offer a scientific explanation of the phenomena.

The instability regions shown in Figures 9 and 10 are curved because β_p (which participates in the combination) is a function of $\varepsilon\gamma$ and k_p. When k_p increases in value the width of the unstable regions tend to decrease as shown in Figure 9. However, the same instability regions often curve downward with increasing k_p, which means that the resonance will be destabilized at a lower speed. Similar behaviour can be observed from the instability regions that curve with mass in Figure 10.

It should be emphasized that the preceding analysis was based on an assumption that throughout its motion the mass has an in-plane velocity $(\dot{\varphi} + \tilde{\Omega})$ which remains within the range of the negatively sloping friction. It is well-known (from physical studies) that at higher velocities $(\dot{\varphi} + \tilde{\Omega})$ the slope of the friction–velocity curve will change its direction to become positive so that the resonances initiated by the in-plane system would cease to exist. This is most likely to occur with those resonances at higher rotational speeds $\tilde{\Omega}$ (i.e., the instability regions at the top of Figures 7–10). In any case the analysis given in this paper is conservative because it relates to the most serious case of practically important conditions where the slope remains negative.

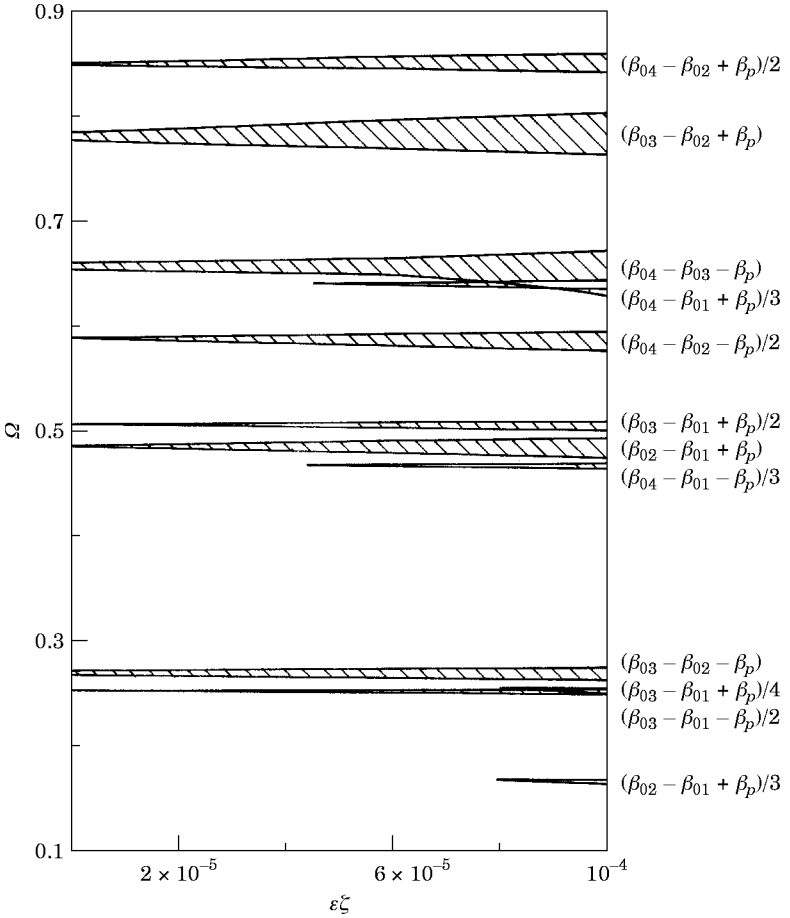

Figure 8. As Figure 7 but dependence on transverse viscous damping $\varepsilon\xi$. $\varepsilon\gamma = 0{\cdot}24$, $\varepsilon\kappa = 0{\cdot}7$, $\varepsilon\xi = 5 \times 10^{-13}$, $\alpha = 3 \times 10^{-5}$, $k_p = 5 \times 10^6$, $\epsilon f = 5 \times 10^{-5}$.

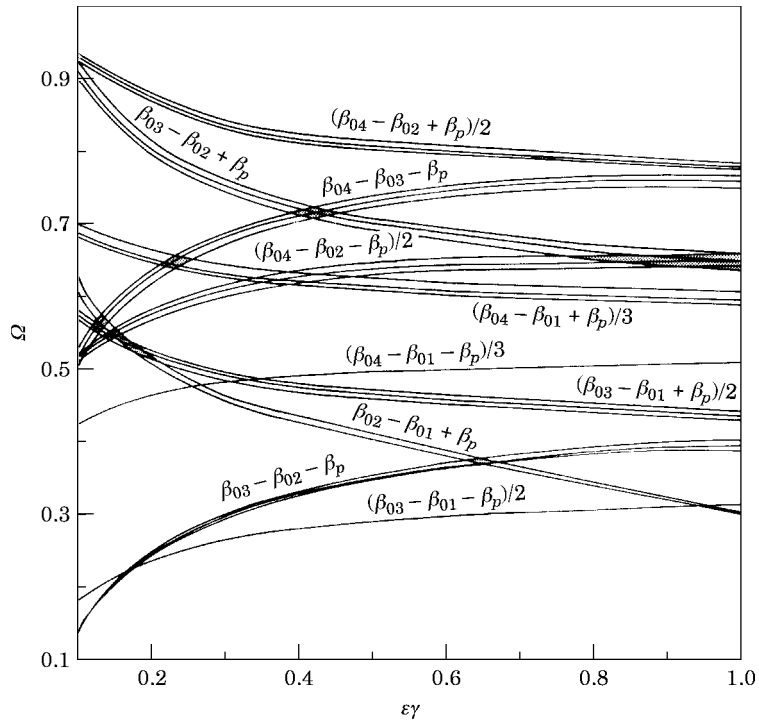

Figure 9. As Figure 7 but dependence on mass $\varepsilon\gamma$. $\varepsilon\kappa = 0{\cdot}7$, $\varepsilon\zeta = 5 \times 10^{-5}$, $\varepsilon\xi = 5 \times 10^{-13}$, $\varepsilon f = 5 \times 10^{-5}$, $\alpha = 3 \times 10^{-5}$, $k_p = 5 \times 10^6$.

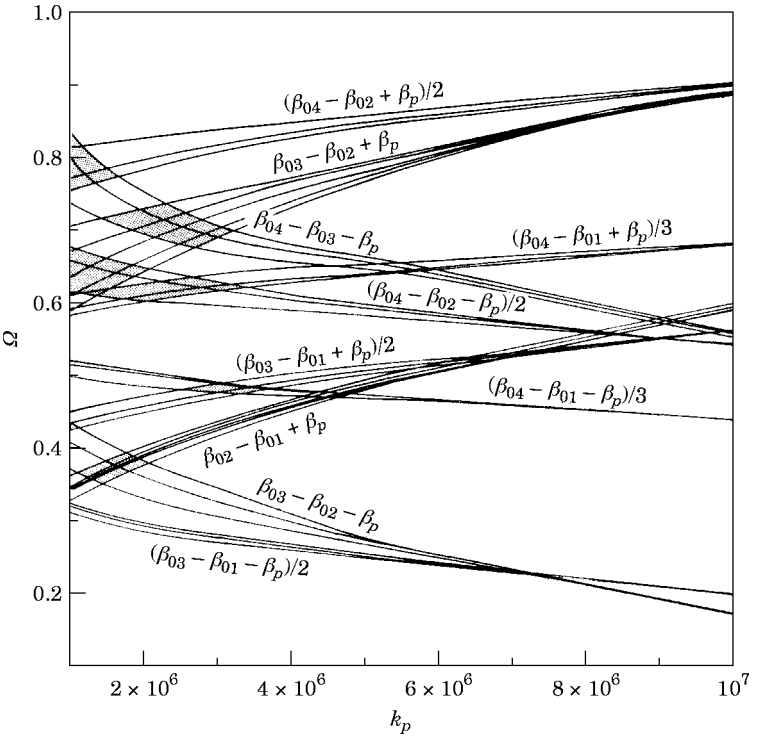

Figure 10. As Figure 7 but dependence on the in-plane stiffness k_p. $\varepsilon\gamma = 0{\cdot}24$, $\varepsilon\kappa = 0{\cdot}7$, $\varepsilon\zeta = 5 \times 10^{-5}$, $\varepsilon\xi = 5 \times 10^{-13}$, $\varepsilon f = 5 \times 10^{-5}$, $\alpha = 3 \times 10^{-5}$.

Although they are mathematically possible, the combinations involving $2\beta_p$ were not studied in this investigation. Very small values for the disc damping, $\varepsilon\xi$, and the slope, α, of the friction–velocity curve were used, which might be considered to counteract each other to some extent.

10. CONCLUSIONS

1. The introduction of an in-plane spring–dashpot and a negative friction–velocity relationship can result in, (i) a modification to the resonances that occur when the friction is constant, and (ii) the initiation of additional resonances.

2. The transverse damper tends to destabilize all the additional resonances.

3. The effect of introducing an in-plane spring–dashpot and a negative friction–velocity relationship is to reduce the regions of instability of the existing resonances.

4. The instabilities of the existing resonances are insensitive to the in-plane spring over a wide range of values.

5. The resonances initiated by the in-plane spring–dashpot and negative friction–velocity relationship are characterized by curved instability regions in the Ω versus $\varepsilon\gamma$ and Ω versus k_p planes. In many cases the resonances will occur at lower speeds when either (or both) $\varepsilon\gamma$ and k_p are increased.

6. The disk damping is stabilizing in all circumstances.

ACKNOWLEDGMENTS

This research is supported by EPSRC (Grant J35177) and BBA Friction Ltd.

REFERENCES

1. C. D. Mote 1970 *Journal of the Franklin Institute* **290**, 329–344. Stability of circular plates subjected to moving loads.
2. C. D. Mote 1977 *Journal of the Acoustical Society of America* **61**, 439–447. Moving-load stability of a circular plate on a floating central collar.
3. W. D. Iwan and K. J. Stahl 1973 *Transactions of the American Society of Mechanical Engineers*, *Journal of Applied Mechanics* **40**, 445–451. The response of an elastic disk with a moving mass system.
4. W. D. Iwan and T. L. Moeller 1976 *Transactions of the American Society of Mechanical Engineers*, *Journal of Applied Mechanics* **43**, 485–490. The response of a spinning disk with a transverse load system.
5. S. G. Hutton, S. Chonan and B. F. Lehman 1987 *Journal of Sound and Vibration* **112**, 527–539. Dynamic response of a guided circular saw.
6. I. Y. Shen and C. D. Mote 1991 *Journal of Sound and Vibration* **148**, 307–318. On the mechanisms of instability of a circular plate under a rotating spring-mass-dashpot system.
7. I. Y. Shen and C. D. Mote 1992 *International Journal of Solids and Structures* **29**, 1019–1032. Parametric excitation under multiple excitation parameters: asymmetric circular plates under a rotating spring.
8. I. Y. Shen 1993 *Transactions of the American Society of Mechanical Engineers*, *Journal of Vibration and Acoustics* **115**, 65–69. Response of a stationary damped circular plate under a rotating slider bearing system.
9. K. Ono, J. S. Chen and D. B. Bogy 1991 *Transactions of the American Society of Mechanical Engineers*, *Journal of the Applied Mechanics* **58**, 1005–1014. Stability analysis of the head–disk interface in a flexible disc drive.
11. J. E. Mottershead and S. N. Chan 1995 *Transactions of the American Society of Mechanical Engineers*, *Journal of Vibration and Acoustics* **117**, 161–163. Flutter instability of circular discs with frictional followers loads.

12. S. N. Chan, J. E. Mottershead and M. P. Cartmell 1994 *Proceedings of the Institution of Mechanical Engineers*, *Part C* **208**, 417–425. Parametric resonances at subcritical speeds in discs with rotating frictional loads.
13. J. E. Mottershead, H. Ouyang, M. P. Cartmell and M. I. Friswell 1997 *Proceedings of the Royal Society of London A* **453**, 1–19. Parametric resonances in an annular disc, with a rotating system of distributed mass and elasticity; and the effects of friction and damping.
14. J. E. Mottershead Vibrations and friction-induced instability in discs *Shock and Vibration Digest* (in press).
15. J. T. Oden and J. A. C. Martins 1985 *Computational Methods in Applied Mechanical Engineering* **52**, 527–634. Models and computational methods for dynamic friction phenomena.
16. B. Armstrong-Helouvry 1991 *Control of Machines with Friction*. Dordrecht: Kluwer.
17. R. A. Ibrahim 1994 *Transactions of the American Society of Mechanical Engineers*, *Applied Mechanics Review* **47**, 209–226. Friction-induced vibration, chatter, squeal, and chaos—Part I: mechanics of contact and friction.
18. R. A. Ibrahim 1994 *Transactions of the American Society of Mechanical Engineers*, *Applied Mechanics Review* **47**, 227–253. Friction-induced vibration, chatter, squeal, and chaos—Part II: dynamics and modelling.
19. H. Ouyang, J. E. Mottershead, M. P. Cartmell and M. I. Friswell (1997) In-plane stick–slip vibration on the surface of a flexible disc clamped between elastic sliders. *Transactions of the American Society of Mechanical Engineers*, 16*th Biennial Conference on Vibration and Noise*, *Sacramento*.
20. A. H. Nayfeh and D. T. Mook 1979 *Nonlinear Oscillations*. New York: Wiley Interscience.

APPENDIX: STABILITY OF RESONANCES INITIATED BY THE IN-PLANE SYSTEM

There are many possible forms of possible parametric combination resonances involving β_p. If the disc is considered to be more rigid than k_p one may assume β_p to be smaller than $\beta_{kl} < \beta_{rs}$ $(k \leqslant r, l < s)$. This assumption reduces the number of resonances, which may appear in any of the following combinations:

$$(s-l)\Omega \approx \beta_{kl} - \beta_{rs} + \beta_p; \qquad (s-l)\Omega \approx \beta_{kl} + \beta_{rs} - \beta_p; \qquad (s-l)\Omega \approx \beta_{rs} - \beta_{kl} - \beta_p;$$

$$(s-l)\Omega \approx \beta_{rs} - \beta_{kl} + \beta_p; \qquad (s+l)\Omega \approx \beta_{kl} - \beta_{rs} + \beta_p; \qquad (s+l)\Omega \approx \beta_{kl} + \beta_{rs} - \beta_p;$$

$$(s+l)\Omega \approx \beta_{rs} - \beta_{kl} - \beta_p; \quad (s+l)\Omega \approx \beta_{rs} - \beta_{kl} + \beta_p; \quad 2l\Omega \approx \beta_p\,; \quad 2l\Omega \approx 2\beta_{kl} - \beta_p;$$

$$(s-l)\Omega \approx \beta_{kl} - \beta_{rs} + 2\beta_p; \qquad (s-l)\Omega \approx \beta_{kl} + \beta_{rs} - 2\beta_p; \qquad (s-l)\Omega \approx \beta_{rs} - \beta_{kl} - 2\beta_p;$$

$$(s-l)\Omega \approx \beta_{rs} - \beta_{kl} + 2\beta_p; \qquad (s+l)\Omega \approx \beta_{kl} - \beta_{rs} + 2\beta_p; \qquad (s+l)\Omega \approx \beta_{kl} + \beta_{rs} - 2\beta_p;$$

$$(s+l)\Omega \approx \beta_{rs} - \beta_{kl} - 2\beta_p; \quad (s+l)\Omega \approx \beta_{rs} - \beta_{kl} + 2\beta_p;$$

$$2l\Omega \approx 2\beta_p; \quad 2l\Omega \approx 2(\beta_{kl} - \beta_p).$$

Formulas for σ for three of them are as follows

Case 1: When $(s-l)\Omega$ is close to $\beta_{rs} - \beta_{kl} + \beta_p$. Suppose that $(s-l)\Omega = \beta_{rs} - \beta_{kl} + \beta_p + \varepsilon\sigma$ so that

$$[(s-l)\Omega - \beta_{rs} - \beta_p]T_0 = -\beta_{kl}\,T_0 + \varepsilon T_1, \qquad [(s-l)\Omega + \beta_{kl} - \beta_p]T_0 = \beta_{rs}\,T_0 + \varepsilon T_1, \tag{A1, A2}$$

The secular terms are eliminated from equation (19) when

$$-\mathrm{i}\beta_{kl}\,(2D_1 + \xi\beta_{kl}^2)\,[A_{kl}\exp(\mathrm{i}\beta_{kl}\,T_0) - B_{kl}\exp(-\mathrm{i}\beta_{kl}\,T_0)] + s\Omega\alpha\varphi_0\,\omega_p$$
$$\times\, R_{kl}\,(r_0)R_{rs}\,(r_0)\,[\mathrm{i}\gamma(\beta_p\,/2 + C_{rs}^{-}) - (\zeta + f\alpha\omega_{cr})/2]B_{rs}\exp[\mathrm{i}(\sigma T_1 - \beta_{kl}\,T_0)] = 0 \tag{A3}$$

and

$$-\mathrm{i}\beta_{rs}\,(2D_1+\xi\beta_{rs}^2)\,[A_{rs}\exp(\mathrm{i}\beta_{rs}\,T_0)-B_{rs}\exp(-\mathrm{i}\beta_{rs}\,T_0)]+l\Omega\alpha\varphi_0\,\omega_p \times R_{kl}(r_0)R_{rs}(r_0)\,[\mathrm{i}\gamma(\beta_p/2-C_{kl}^-)+(\zeta+f\alpha\omega_{cr})/2]B_{kl}\exp[-\mathrm{i}(\beta_{rs}\,T_0+\sigma T_1)]=0 \tag{A4}$$

which leads to

$$\mathrm{i}\beta_{kl}\,(2\mathrm{i}\lambda+\xi\beta_{kl}^2)b_{kl}+s\Omega\alpha\varphi_0\,\omega_p\,R_{kl}(r_0)R_{rs}(r_0)\,[\mathrm{i}\gamma(\beta_p/2+C_{rs}^-)-(\zeta+f\alpha\omega_{cr})/2]b_{rs}=0 \tag{A5}$$

and

$$l\Omega\alpha\varphi_0\,\omega_p\,R_{kl}(r_0)R_{rs}(r_0)\,[\mathrm{i}\gamma(\beta_p/2-C_{kl}^-)+(\zeta+f\alpha\omega_{cr})/2]b_{kl}+\mathrm{i}\beta_{rs}\,[2\mathrm{i}(\lambda-\sigma)+\xi\beta_{rs}^2)b_{rs}=0 \tag{A6}$$

when

$$B_{kl}=b_{kl}\exp(\mathrm{i}\lambda T),\qquad B_{rs}=b_{rs}\exp(\mathrm{i}(\lambda-\sigma)T_1). \tag{A7, A8}$$

The condition for the existence of a non-trivial solution is that the determinant of the coefficient matrix (formed from equations (A5) and (A6)) should vanish, which leads to a quadratic equation in λ, and σ is determined by setting the imaginary part of λ to zero thereby defining the transition from stable to unstable vibrations.

Case 2: When $(s+l)\Omega$ is close to $\beta_{rs}-\beta_{kl}+\beta_p$. The equation which determines the instability regions is found to be

$$\begin{vmatrix} \mathrm{i}\beta_{kl}\,(2\mathrm{i}\lambda+\xi\beta_{kl}^2) & s\Omega\alpha\varphi_0\,\omega_p\,R_{kl}(r_0)R_{rs}(r_0)\left\{\mathrm{i}\gamma\left(\dfrac{\beta_p}{2}+C_{rs}^-\right)+\dfrac{\zeta+f\alpha\omega_{cr}}{2}\right\} \\ l\Omega\alpha\varphi_0\,\omega_p\,R_{kl}(r_0)R_{rs}(r_0)\left\{\mathrm{i}\gamma\left(\dfrac{\beta_p}{2}-C_{kl}^+\right)-\dfrac{\zeta+f\alpha\omega_{cr}}{2}\right\} & -\mathrm{i}\beta_{rs}\,[2\mathrm{i}(\lambda+\sigma)+\xi\beta_{rs}^2) \end{vmatrix}=0. \tag{A9}$$

Case 3: When $(s-l)\Omega$ is close to $\beta_{kl}-\beta_{rs}+2\beta_p$. The equation which determines the instability regions is found to be

$$\begin{vmatrix} \mathrm{i}\beta_{kl}\,(2i\lambda+\xi\beta_{kl}^2) & \dfrac{\gamma(s\Omega\alpha\varphi_0\,\omega_p)^2}{4}\,R_{kl}(r_0)R_{rs}(r_0) \\ \dfrac{\gamma(l\Omega\alpha\varphi_0\,\omega_p)^2}{4}\,R_{kl}(r_0)R_{rs}(r_0) & \mathrm{i}\beta_{rs}\,[2i(\lambda-\sigma)+\xi\beta_{rs}^2] \end{vmatrix}=0. \tag{A10}$$